



Published in final edited form as:

Mech Mater. 2012 January 1; 44: 99–109. doi:10.1016/j.mechmat.2011.07.004.

Lamina Cribrosa Thickening in Early Glaucoma Predicted by a Microstructure Motivated Growth and Remodeling Approach

Rafael Grytz^{*,a}, Ian A. Sigal^b, Jeffrey W. Ruberti^c, Günther Meschke^d, and J. Crawford Downs^a

^aOcular Biomechanics Laboratory, Devers Eye Institute, Portland, Oregon

^bDepartment of Ophthalmology, University of Pittsburgh, Pittsburgh, Pennsylvania

^cExtracellular Matrix Engineering Research Laboratory, Mechanical and Industrial Engineering, Northeastern University, Boston, Massachusetts

^dInstitute of Structural Mechanics, Ruhr-University Bochum, Bochum, Germany

Abstract

Glaucoma is among the leading causes of blindness worldwide. The ocular disease is characterized by irreversible damage of the retinal ganglion cell axons at the level of the lamina cribrosa (LC). The LC is a porous, connective tissue structure whose function is believed to provide mechanical support to the axons as they exit the eye on their path from the retina to the brain. Early experimental glaucoma studies have shown that the LC remodels into a thicker, more posterior structure which incorporates more connective tissue after intraocular pressure (IOP) elevation. The process by which this occurs is unknown. Here we present a microstructure motivated growth and remodeling (G&R) formulation to explore a potential mechanism of these structural changes. We hypothesize that the mechanical strain experienced by the collagen fibrils in the LC stimulates the G&R response at the micro-scale. The proposed G&R algorithm controls collagen fibril synthesis/degradation and adapts the residual strains between collagen fibrils and the surrounding tissue to achieve biomechanical homeostasis. The G&R algorithm was applied to a generic finite element model of the human eye subjected to normal and elevated IOP. The G&R simulation underscores the biomechanical need for a LC at normal IOP. The numerical results suggest that IOP elevation leads to LC thickening due to an increase in collagen fibril mass, which is in good agreement with experimental observations in early glaucoma monkey eyes. This is the first study to demonstrate that a biomechanically-driven G&R mechanism can lead to the LC thickening observed in early experimental glaucoma.

Keywords

Glaucoma; Lamina Cribrosa; Growth; Remodeling; Residual Strains; Crimped Collagen Fibrils; Optic Nerve Head

© 2011 Elsevier Ltd. All rights reserved.

*Corresponding author rafael@grytz.de (Rafael Grytz).

Publisher's Disclaimer: This is a PDF file of an unedited manuscript that has been accepted for publication. As a service to our customers we are providing this early version of the manuscript. The manuscript will undergo copyediting, typesetting, and review of the resulting proof before it is published in its final citable form. Please note that during the production process errors may be discovered which could affect the content, and all legal disclaimers that apply to the journal pertain.

1. Introduction

Glaucoma is a leading cause of blindness in the world and is due to the loss of retinal ganglion cell axons. These axons deteriorate in a region in the posterior pole of the eye known as the optic nerve head (ONH). The axons pass through the lamina cribrosa (LC) as they exit the eye at the ONH. The LC is characterized by a porous, connective tissue structure composed of lamellar beams. The function of the LC is unclear, but is believed to include providing mechanical support to the axons within the ONH region. Experiments have shown that inducing elevated intraocular pressure (IOP) leads to many of the structural changes in the eye associated with early stages of glaucoma (Figures 1, 2). It has been shown that chronic intraocular IOP elevations in monkey eyes result in several structural changes in the LC: (i) overall thickening of the LC (20 to 61 μm , Yang et al., 2007, 2011); (ii) increased LC excavation (25 to 233 μm , Yang et al., 2007, 2011); (iii) increase in connective tissue volume (44% to 82%, Roberts et al., 2009); (iv) increased number of lamellar beams through the LC thickness (17% to 48%, Roberts et al., 2009); (v) outward migration of the posterior lamina insertion point (Yang et al., 2010); and (vi) less pronounced outward migration of the anterior lamina insertion point (Yang et al., 2010). These structural changes are assumed to play an important role in the pathophysiology of glaucoma, where elevated IOP is known to be the most relevant risk factor. In this paper we present an initial approach to computationally predict the bio-mechanical need for a LC in humans and to simulate the G&R process of the LC during the development of glaucoma.

The aim of this paper is to derive a computational G&R formulation capable of predicting the structural changes seen in the earliest stage of experimental glaucoma. In the last decade many computational formulations have been developed to model finite growth of soft tissues (Epstein and Maugin, 2000; Lubarda and Hoger, 2002; Göktepe et al., 2010; Himpel et al., 2005; Klisch et al., 2003; Kuhl et al., 2007), and their findings were recently summarized by Ambrosi et al. (2011). While existing numerical models can simulate finite growth of soft tissues by means of the kinematic growth of finite elements, to the best knowledge of the authors, tissue recruitment across finite element borders has not been modeled. This is important because tissue recruitment is believed to be a key component of the G&R process of the LC during the earliest stages of glaucoma (Roberts et al., 2009; Yang et al., 2010; Downs et al., 2010). To numerically model tissue recruitment, a mixture-based constitutive formulation is incorporated and the growth process is consistently introduced at both the kinematic and constitutive levels in accordance with the work of Schmid et al. (2011). Tissue growth is thus the result of a balance between the synthesis and degradation of collagen fibrils. Note that our model has a fundamental difference from previous work in that we do not presuppose the existence of a LC. The model allows for collagen fibrils to develop anywhere within the neural canal (or not). Thus the existence of a region with high collagenous content, which we identify as LC, is a prediction of the model and not an assumption.

Most existing formulations motivate the G&R process from an imbalance in mechanical stress or strain at the macro-scale. Flynn et al. (2010) showed recently that the mechanical strain experienced by the collagen fibrils protects the fibrils against enzymatic degradation by matrix metalloproteinases. We thus propose a stimulus function consistent with this experimental finding, where the G&R process is driven by the mechanical stretch experienced by collagen fibrils at the micro-level. The collagen fibril stretch is assumed to differ from the tissue stretch measured at the macro-scale due to residual strains (Watton et al., 2009b) and collagen fibril crimping (Grytz and Meschke, 2009). Collagen fibrils are constantly removed and deposited in the LC (Yang et al., 1993), which in turn may introduce residual strains between collagen fibrils and the surrounding bulk tissue. Similar to Watton et al. (2009b), we propose a remodeling rule for the adaptation of the residual stretch

between collagen fibrils and the bulk tissue material in addition to the changing collagen fibril mass.

In Section 2 of this manuscript we present the theoretical framework of the proposed G&R algorithm. In Section 3 we apply the algorithm to a generic finite element model of the human eye. We conclude in Section 4 with a discussion of the algorithm, the results and the model limitations.

2. Lamina Cribrosa Growth and Remodeling

In this section a G&R approach is derived to simulate the structural changes of the LC seen during the earliest stages of experimental glaucoma. The LC is traditionally defined by its porous collagen architecture through which axon bundles exit the eye. Astrocytes and other cells are present to maintain the tissue functionality. We assume that the LC tissue volume includes three constituents, which we treat as solids: (i) the collagen fibril architecture (col); (ii) the axon bundles (axon) and (iii) the surrounding matrix material (mat), which includes cells, elastin and other extracellular matrix components. Collagen fibrils are thought to be constantly removed and deposited in the LC. We hypothesize that an upregulated synthesis or downregulated degradation of collagen fibrils may alter the collagen content and cause the volumetric growth of collagenous tissues (Laurent et al., 1985, 1978; Bhole et al., 2009). The thickening of the LC seen in early experimental glaucoma is thus assumed to be a consequence of collagen fibril mass increase stimulated by the elastic stretch experienced by the collagen fibril material.

2.1. Growth and Remodeling Stimulus

In accordance with Flynn et al. (2010); Bhole et al. (2009); Camp et al. (2011), we hypothesize that the elastic stretch λ^{fib} experienced by the collagen fibril material will stimulate the G&R response of the LC. The proposed stimulus is based on the idea that G&R occurs in an effort to maintain a homeostatic elastic stretch environment λ^{hom} at the collagen fibril level $\lambda^{\text{fib}} \rightarrow \lambda^{\text{hom}}$. We define the G&R stimulus function as

$$\phi = \lambda^{\text{fib}} - \lambda^{\text{hom}}, \quad (1)$$

where the homeostatic state is represented by $\phi = 0$. It is unclear how deviations from this homeostatic state are sensed and eventually trigger the changes that result in the tissue's attempt to restore homeostasis.

2.2. Collagen Fibril Crimp and Residual Strains

At the micro-scale, collagen fibrils may crimp or buckle. We derived the constitutive response of a helically crimped collagen fibril in Grytz and Meschke (2009) and estimated its 1-dimensional strain energy contribution $W^{\text{fib}}(\lambda^{\text{axial}})$ as a function of the axial stretch of the helix. The collagen fibril will uncrimp and stretch when subjected to a load in the axial direction \mathbf{e}_0 of the helix. Within the crimped collagen fibril model the axial stretch is multiplicatively decomposed into a part λ^{crimp} representing the geometrical (un-)crimping of the fibril and the elastic stretch of the fibril material λ^{fib} (see equation 21 in Grytz and Meschke, 2009)

$$\lambda^{\text{axial}} = \lambda^{\text{fib}} \lambda^{\text{crimp}}. \quad (2)$$

Collagen fibril turnover may lead to residual strains between the collagen fibrils and its surrounding matrix material. Therefore, we introduce the residual stretch λ_R that links the axial stretch λ^{axial} of the crimped collagen fibril to the elastic stretch experienced by the

surrounding matrix material λ^{mat} and the axon bundles λ^{axon} , which are assumed to undergo the same level of deformation that can be measured at the macro-scale λ_e

$$\lambda_e = \lambda^{\text{mat}} = \lambda^{\text{axon}} = \lambda_R \lambda^{\text{axial}}. \quad (3)$$

Note that the residual stretch λ_R is similar to the recruitment stretch previously introduced by Watton et al. (2009b). Therefore, the residual stretch can be interpreted as the macroscopic stretch level that the bulk tissue (and the axons, matrix material) must undergo in the in the direction of the collagen fibril for it to bear tensile load. However, in contrast to Watton et al. (2009b), we assume that collagen fibrils can bear load under compression. It is unclear if collagen fibrils embedded in soft tissues can bear load under compression. However, the stiffness response of the helical crimp model is very soft in these states without loss of convexity (Grytz and Meschke, 2009).

Figure 3 illustrates the implication of equations (2) and (3). The residual stretch is only required to be positive $\lambda_R > 0$. According to (2), the axial stretch of the collagen fibril λ^{axial} may be lower or higher compared to the macroscopic elastic stretch λ_e due to residual strains. In contrast, the crimping stretch is bounded by the axial stretch ($1 \leq \lambda^{\text{crimp}} < \lambda^{\text{axial}} \quad \forall \quad \lambda^{\text{axial}} > 1$ and $\lambda^{\text{axial}} > \lambda^{\text{crimp}} \geq 1 \quad \forall \quad \lambda^{\text{axial}} > 1$) and by the so called locking stretch ($\lambda^{\text{crimp}} < \lambda_{\text{lock}} = 1/\cos\theta_0$) through the boundary value problem at the micro-level (Grytz and Meschke, 2009). Consequently, the absolute strain level experienced by the collagen fibril material is always lower compared to the absolute strain in the fibril's axial direction $|\lambda^{\text{fib}} - 1| < |\lambda^{\text{axial}} - 1|$.

It is often suggested that residual strains evolve mainly due to the continuous synthesis and degradation of collagen fibrils while the tissue is subjected to external loading (Machyshyn et al., 2010). Foolen et al. (2010) demonstrated that chicken embryo periosteum resides in a homeostatic mechanical state, which is characterized by a residual strain that corresponds to the to the end of the toe and the beginning of the heel region of the stress-strain curve of the tissue. They demonstrated that this homeostatic state was regained upon strain perturbation. In contrast to the common assumption, this remodeling phenomena did not depend on protein synthesis, because the addition of cycloheximide did not affect the response. In view of this evidence, we decided to formulate an independent evolution equation for the residual stretch λ_R rather than relating it to the collagen fibril synthesis and degradation derived in the following subsection. We propose a simple linear differential equation for the evolution of λ_R

$$\dot{\lambda}_R = \frac{d\lambda_R}{dt} = \frac{1}{\tau_R} \phi, \quad (4)$$

where the homeostatic mechanical state is defined at the micro-level through the stimulus function ϕ in (1). The parameter τ_R in (4) relates to the remodeling time needed to achieve homeostasis.

2.3. Lamina Cribrosa Thickening

To numerically describe the thickening of the LC seen in early experimental glaucoma, we adopt the concept of finite volumetric growth characterized through the multiplicative split of the deformation gradient \mathbf{F} into an elastic \mathbf{F}_e and an growth part \mathbf{F}_g (Rodriguez et al., 1994)

$$\mathbf{F} = \mathbf{F}_e \mathbf{F}_g. \quad (5)$$

The volume change of a differential volume element is defined by the determinant of \mathbf{F} which can be also split according to (5) into elastic and growth related volume changes

$$J = \frac{dV}{dV_0} = \det \mathbf{F} = \frac{dV}{dV_g} \frac{dV_g}{dV_0} = \det \mathbf{F}_e \det \mathbf{F}_g = J_e J_g. \quad (6)$$

Here, the volume elements dV , dV_g and dV_0 relate to the current configuration \mathcal{B} , the grown (or intermediate) configuration \mathcal{B}_g and the reference configuration \mathcal{B}_0 of the LC tissue.

Let \mathbf{M}_i be an orthonormal basis defined in the reference configuration of the body \mathcal{B}_0 , where \mathbf{M}_3 points into the thickness direction of the LC. A dedicated thickening of the LC can be introduced by specifying the growth tensor as follows

$$\mathbf{F}_g = \mathbf{I} + (\lambda_g - 1) \mathbf{M}_3 \otimes \mathbf{M}_3, \quad (7)$$

where λ_g represents a growth multiplier of the tissue volume. Pure elastic deformations are represented by $\lambda_g = 1$ while LC shrinkage occur for $\lambda_g < 1$ and LC thickening for $\lambda_g > 1$. One can easily relate the Jacobian of the growth tensor to the growth multiplier as

$$J_g = \det \mathbf{F}_g = \lambda_g. \quad (8)$$

2.4. Lamina Cribrosa Constituents

Following the volume fractions concept, we introduce the initial volume fractions n_0^α , which refer the volume element dV_0^α of each of the three considered constituents ($\alpha = \text{col, axon, mat}$) to the bulk tissue volume element dV_0 at the initial configuration \mathcal{B}_0

$$n_0^\alpha = \frac{dV_0^\alpha}{dV_0}. \quad (9)$$

The volume occupied by collagen fibrils may change due to changes in collagen fibril synthesis or degradation as will be derived in Subsection 2.5. This change in collagen fibril volume from the initial \mathcal{B}_0 to the (intermediate) grown configuration \mathcal{B}_g is represented by the growth Jacobian

$$J_g^{\text{col}} = \frac{dV_g^{\text{col}}}{dV_0^{\text{col}}}. \quad (10)$$

Following the derivations of Schmid et al. (2011) the volumetric growth of the bulk material J_g (8) can be redefined by the growth Jacobians of its constituents $J_g^\alpha = dV_g^\alpha / dV_0^\alpha$

$$J_g = \frac{dV_g}{dV_0} = \sum_\alpha \frac{dV_g^\alpha}{dV_0^\alpha} = \sum_\alpha \frac{dV_g^\alpha}{dV_0^\alpha} \frac{dV_0^\alpha}{dV_0} = \sum_\alpha J_g^\alpha n_0^\alpha \quad (11)$$

Equation (11) can be further simplified as we assume that the volume occupied by the axon bundles and the matrix material remain constant during the growth process $J_g^{\text{axon}} = J_g^{\text{mat}} = 1$

$$J_g = J_g^{\text{col}} n_0^{\text{col}} + n_0^{\text{axon}} + n_0^{\text{mat}}. \quad (12)$$

Note that relation (12) links the volume change of the collagen fibril architecture (10) to the kinematic thickening of the LC bulk material (7) through (8) (see illustration in Figure 4).

Changes in the volume occupied by the collagen fibril architecture (10) will lead to a new mixture with modified volume fractions for all three constituents. At the grown configuration the volume fractions can be derived from (9), (10) and (11)

$$n_g^\alpha = \frac{dV_g^\alpha}{dV_g} = \frac{n_g^\alpha}{n_0^\alpha} n_0^\alpha = \frac{dV_g^\alpha}{dV_0^\alpha} \frac{dV_0^\alpha}{dV_g} n_0^\alpha = \frac{J_g^\alpha}{J_g} n_0^\alpha. \quad (13)$$

Note that at any time the sum of volume fractions satisfies the volume fraction condition:

$$n_0^{\text{col}} + n_0^{\text{axon}} + n_0^{\text{mat}} = n_g^{\text{col}} + n_g^{\text{axon}} + n_g^{\text{mat}} = 1. \quad (14)$$

2.5. Collagen Fibril Synthesis and Degradation

Experimental studies revealed that the mechanical environment of soft tissues may impact both the synthesis and degradation of collagen fibrils (Flynn et al., 2010; Wang and Thampatty, 2006). Due to changes in collagen fibril synthesis and degradation, the number of collagen fibrils per unit bulk volume may change from N_0^{fib} at time t_0 to N^{fib} at time t . If the mass of one collagen fibril m_0^{fib} remains constant in time, the change in collagen fibril mass density may be approximated by the change in the volume occupied by the collagen fibril architecture as assumed here

$$\frac{N^{\text{fib}} m_0^{\text{fib}}}{N_0^{\text{fib}} m_0^{\text{fib}}} \approx \frac{dV_g^{\text{col}}}{dV_0^{\text{col}}} = J_g^{\text{col}}. \quad (15)$$

We introduce a simple evolution equation for the growth Jacobian of the collagen fibril architecture J_g^{col} to model the changing collagen fibril synthesis and degradation stimulated by the criterion ϕ (1)

$$\dot{J}_g^{\text{col}} = \frac{dJ_g^{\text{col}}}{dt} = k^{\text{col}} \phi. \quad (16)$$

The volumetric growth in collagen fibrils is weighted by the function k^{col}

$$k^{\text{col}}(J_g^{\text{col}}) = \frac{1}{\tau_g} \left[\frac{J_{g,\text{max}}^{\text{col}} - J_g^{\text{col}}}{J_{g,\text{max}}^{\text{col}} - 1} \right]^2 \left[\frac{J_g^{\text{col}} - J_{g,\text{min}}^{\text{col}}}{1 - J_{g,\text{min}}^{\text{col}}} \right]^2 \quad (17)$$

where τ_g relates to the turnover rate of collagen fibrils. To assure the functionality of the LC, we assume that the volumetric growth in collagen fibrils is constrained such that enough volume is left for the axon bundles to pass through the collagen fibril architecture and that not all collagen fibrils vanish. Therefore, the volumetric growth in collagen fibrils (16) is

bounded by the maximal $J_{g,\text{max}}^{\text{col}}$ and the minimal volume change $J_{g,\text{min}}^{\text{col}}$ in (17). Note that while the stimulus ϕ in the evolution equation (16) is based on the microstructure of collagen fibrils, the weighting function k^{col} is phenomenologically motivated.

As proposed by Watton et al. (2009b), we assume that collagen fibrils are prestretched after synthesis and this prestretch (or attachment stretch) level is identical to the homeostatic stretch level λ^{hom} . Note that this assumption allows for a constant collagen turnover rate at

homeostasis without activating the G&R stimulus (1) or changing the constitutive response of the tissue.

2.6. Constitutive Equations

The increase or decrease in collagen fibril mass will change the composition of LC constituents and, therefore, also impact the strain energy density of the LC bulk material W . We assume that the strain energy contribution W^α of each constituent ($\alpha = \text{col, axon, mat}$) is linearly dependent on its volume fraction n_g^α defined at the grown configuration \mathcal{B}_g

$$W = \sum_{\alpha} n_g^\alpha W^\alpha + U, \quad (18)$$

where U represents the volumetric energy contribution of the bulk material. The tissue strain energy density can be reformulated by using (13) and incorporating the growth Jacobian of the collagen architecture J_g^{col} and the bulk LC material J_g

$$\begin{aligned} W &= \sum_{\alpha} \frac{n_g^\alpha}{n_0^\alpha} n_0^\alpha W^\alpha + U = \sum_{\alpha} \frac{J_g^\alpha}{J_g} n_0^\alpha W^\alpha + U \\ &= \frac{J_g^{\text{col}}}{J_g} n_0^{\text{col}} W^{\text{col}} + \frac{n_0^{\text{axon}}}{J_g} W^{\text{axon}} + \frac{n_0^{\text{mat}}}{J_g} W^{\text{mat}} + U. \end{aligned} \quad (19)$$

Let us assume that the strain energy density W stored in the tissue can be characterized in terms of the elastic right Cauchy-Green tensor

$$\mathbf{C}_e = \mathbf{F}_e^T \mathbf{F}_e = \mathbf{F}_g^{-T} \mathbf{C} \mathbf{F}_g^{-1}. \quad (20)$$

It was previously shown that the second Piola-Kirchhoff stress \mathbf{S} is thermodynamically conjugated to the right Cauchy-Green tensor $\mathbf{C} = \mathbf{F}^T \mathbf{F}$ and can be interpreted as the pull back of the elastic stress tensor \mathbf{S}_e from the grown configuration \mathcal{B}_g to the reference configuration \mathcal{B}_0

$$\mathbf{S} = 2 \frac{\partial W(\mathbf{C}_e)}{\partial \mathbf{C}} = \mathbf{F}_g^{-1} \mathbf{S}_e \mathbf{F}_g^{-T} \quad \text{with} \quad \mathbf{S}_e = 2 \frac{\partial W(\mathbf{C}_e)}{\partial \mathbf{C}_e}. \quad (21)$$

For detailed derivations and extensive discussions on open system thermodynamics we refer to the literature (Epstein and Maugin, 2000; Lubarda and Hoger, 2002; Kuhl and Steinmann, 2003; Himpel et al., 2005).

The strain energy function of the matrix material is approximated by means of an isochoric Neo-Hookean formulation

$$W^{\text{mat}}(\mathbf{C}_e) = \frac{1}{2} \mu \left(J_e^{-2/3} \text{tr} \mathbf{C}_e \right) \quad (22)$$

with the shear modulus μ . While the isochoric energy contribution of the axon bundles is assumed to be negligible $W^{\text{axon}} = 0$, its volumetric contribution is indirectly considered through U representing the volumetric response of the bulk material of the mixture

$$U(J_e) = \frac{1}{2} K (\ln J_e)^2, \quad (23)$$

where K is the bulk modulus.

Following our previous work (Grytz, 2008; Grytz and Meschke, 2010), the collagen fibril architecture is represented by a generalized structure tensor

$$\mathbf{H} = \kappa \mathbf{M}_1 \otimes \mathbf{M}_1 + (1 - \kappa) \mathbf{M}_2 \otimes \mathbf{M}_2. \quad (24)$$

where collagen fibril orientations \mathbf{e}_0 were assumed to be normally distributed around the preferred direction \mathbf{M}_1 in the plane spanned by \mathbf{M}_1 and \mathbf{M}_2 . The mesostructural parameter $\kappa \in [0; 0.5]$ represents the collagen fibril dispersion in an integral sense. Roberts et al. (2009) reported that the anisotropic collagen fibril dispersion of the LC does not change during early experimental glaucoma. Accordingly, the generalized structure tensor (24) is assumed to be constant in time.

If we, furthermore, assume constant residual stretch values λ_R in all fibril orientation \mathbf{e}_0 , the overall elastic stretch of the collagen architecture can be approximated as

$$\lambda^{\text{col}} \approx \frac{\sqrt{\mathbf{C}_e \cdot \mathbf{H}}}{\lambda_R} = \frac{\sqrt{\mathbf{C} \cdot \mathbf{H}}}{\lambda_R}. \quad (25)$$

Note that due to the dedicated growth of the LC in its thickness direction \mathbf{M}_3 assumed by the growth tensor in (7), the elastic stretch of the collagen architecture can be directly computed by using \mathbf{C} in (25). The strain energy contribution of the collagen architecture is approximated by the energy function derived in Grytz and Meschke (2009) for one crimped collagen fibril as a function of the overall collagen stretch

$$W^{\text{col}} = W^{\text{fib}}(\lambda^{\text{axial}}) \quad (26)$$

with $\lambda^{\text{axial}} = \lambda^{\text{col}}(\mathbf{C}, \mathbf{H}, \lambda_R)$ according to (25). The strain energy density function W^{fib} cannot be presented in a closed form, but a detailed derivation can be found in Grytz and Meschke (2009). Note that the solution of (26) will provide both the current constitutive response of the collagen fibril architecture and the collagen fibril stretch λ_{fib} used in (1) to define the G&R stimulus.

3. Numerical Example

The G&R formulation presented in Section 2.1 is now applied to a generic, axisymmetric finite element model of the human ONH.

3.1. Finite element model of the human optic nerve head

The geometry of the eye model was adapted from a previously described parametric model and includes the sclera, the neural canal tissues and the pia mater (Figure 5; for dimensions see base-line model in Sigal et al., 2005). The neural tissue anteriorly to the modeled neural canal tissues was assumed to be unable to incorporate a LC-like structure and was therefore disregarded in the model. A 10° piece of the axisymmetric eye model was discretized into 4002 hexahedral finite elements and standard axisymmetric boundary conditions were applied (Figure 5). The 20-node quadratic element formulation is based on a reduced integration scheme provided by the commercial finite element suite ABAQUS (Ver. 6.8, Hibbitt, Karlsson & Sorensen, Inc., Providence, RI). The collagen architecture in the tissues was represented by the generalized structure tensor (24) and the dispersion parameter κ . In the peripapillary ring region the collagen fibrils were assumed to be perfectly aligned ($\kappa = 0$) surrounding the scleral canal. In the rest of the scleral shell and in the pial sheath the collagen fibrils were assumed to be aligned in-plane with isotropic dispersion within the plane ($\kappa = 0.5$). The tissues of the neural canal were also assumed to have collagen fibrils with planar isotropy ($\kappa = 0.5$) in the extended plane of the sclera. The peripapillary ring of

circumferentially aligned collagen fibrils has been shown histologically (Hernandez et al., 1987; Morrison et al., 1989) and by using second harmonic imaging techniques (Winkler et al., 2010). The biomechanical advantages of the peripapillary fibril ring and its important implication on the stress environment of LC were previously discussed in Grytz et al. (2011); Girard et al. (2009).

The strain energy contributions W^{col} and W^{mat} were assumed to represent the energy contribution of basic tissue constituents, in particular, the collagen fibril architecture and its surrounding matrix material. Consequently, the constitutive parameters of W^{mat} and W^{col} summarized in Table 1 were assumed to be constant in all the tissues of the eye model and tissue-specific differences in the hyperelastic response were exclusively introduced by tissue-specific volume fractions and the collagen fibril dispersion. To avoid numerical instabilities due to volume locking, the eye tissues were considered as slightly compressible. The bulk modulus was set to 0.2 MPa for the neural canal tissues and 2.0 MPa for the other tissues. The initial volume fractions are summarized in Table 2.

The G&R rules outlined in Section 2.1 were exclusively applied to the tissues within the neural canal. Volumetric growth of the collagen fibril architecture was limited to $J_{g,\text{max}}^{\text{col}}=3.92$ and minimal volume change $J_{g,\text{min}}^{\text{col}}=0.0016$ through (17) thereby restricting the volume fraction of collagen fibrils to be between 20% and 0.01%. The lower limit therefore prevents the algorithm from reaching the singular case of $n_g^{\text{col}}=0$. The data available from the literature indicate that the connective tissue volume fraction in the LC is between 12% and 45%, which includes the laminar capillary volume, cells, and non-fibrillar extracellular matrix components (Roberts et al., 2009). Since the fibrillar components are a fraction of the total LC connective tissue volume, we believe the upper limit of 20% collagen fibril volume fraction is reasonable. The temporal discretization of the evolution equations (4) and (16) was realized by the explicit update of the collagen fibril volume fraction n_g^{col} and the residual stretch λ_R . Due to their phenomenological nature, the time constants controlling the speed of the G&R process are given with respect to arbitrary time units (TU), normalized as follows: $\tau_R = 1.0$ TU and $\tau_g = 0.01$ TU. Time increments were kept reasonably small to prevent numerical oscillation during the G&R simulation. The homeostatic collagen fibril stretch was estimated to $\lambda^{\text{hom}} = 1.001$. This fibril stretch relates to the tissue stretch that corresponds to the end of the toe and the beginning of the heel region of the tissue stress-stretch curve similar to the homeostatic mechanical state in chicken embryo periosteum observed by Foolen et al. (2010).

At $t = t_0 = 0$ the simulation started with a uniform initial collagen fibril content throughout the neural canal tissues and IOP was quasi-instantly increased to a normal value of 15 mmHg. Then, IOP was held constant and the G&R rules were applied until homeostasis was achieved at $t = t_1 = 300$ TU. Thereafter IOP was (quasi instantly) elevated to 25 mmHg. Due to G&R, homeostasis was again achieved at elevated IOP at $t = t_3 = 600$ TU.

3.2. Numerical results

Selected numerical results of the G&R simulation showing the evolution of the LC at time $t = t_0, t_1, t_2$ are presented in Figure 6. We assume that neural canal tissues with a collagen fibril volume fraction n_g^{col} of 10% or more represents the LC, while tissues with less than 10% collagen fibril volume fraction represent pre- and retro-laminar tissue. At $t = t_0$ the normal IOP level (15 mmHg) was applied to the initial eye model considering uniform collagen fibril content throughout the neural canal tissues. Due to the pressure loading, collagen fibrils were overstretched ($\lambda^{\text{fib}} > \lambda^{\text{hom}}$) across the scleral canal as can be seen in bottom left of Figure 6. This in turn stimulated the G&R algorithm to increase collagen fibril

mass across the scleral canal while decreasing it in pre- and retro-laminar regions. At $t = t_1$, all collagen fibrils within the neural canal reached the hypothesized homeostasis and a LC-like structure that spans across the scleral canal was created by the G&R algorithm. The residual stretch was minimal at $t = t_1$.

An IOP elevation to 25 mmHg reactivated the G&R process, which resulted in LC thickening due to the recruitment of pre- and retro-laminar tissues into the LC. Characteristic structural changes of LC that developed during the early glaucoma G&R simulation are presented in Table 3. The LC thickness increased by 50% at the center and 30% at the insertion of the LC into the sclera and pia. This thickening resulted partially from a higher collagen fibril concentration in the core region of the LC but mainly from the recruitment of pre- and retro-laminar tissues into the LC. In total, the collagen fibril volume in the LC increased by 63% from t_1 to t_2 while the LC bulk tissue volume increased by 52%. Residual stretch evolved locally with the maximal value $\lambda_{R,\max} = 1.02$ near the region, where the LC, sclera, pia and optic nerve meet.

4. Discussion and Limitations

A numerical G&R algorithm was presented for soft biological tissues to simulate tissue growth and recruitment induced by changing collagen fibril synthesis and degradation. Tissue recruitment was numerically accomplished by incorporating a mixture-based constitutive formulation and introducing the growth process consistently at both the kinematic and constitutive level as suggested by Schmid et al. (2011).

The proposed G&R algorithm was applied to a generic finite element model of the human ONH with uniform initial collagen content throughout the tissues within the neural canal, and allowed to achieve homeostasis at normal (15 mmHg) and elevated IOP (25 mmHg). At normal IOP, the G&R algorithm created a LC-like structure that spanned the scleral canal and as such provided evidence in support of the biomechanical need for a LC in humans. At elevated IOP, the simulation remodeled the structure of the LC as follows to maintain the hypothesized homeostatic state: (i) 63% increase in collagen fibril volume; (ii) up to 2% increase in local residual strain; (iii) 52% increase in LC volume; (iv) 40% increase in LC thickness; (v) recruitment of pre- and retro-laminar tissues into the LC; (vi) inward migration of the anterior lamina insertion point and (vii) outward migration of the posterior lamina insertion point that resulted in further insertion of the LC into the pia mater (see Fig. 3 for the definition of the anterior and posterior lamina insertion point).

The bulk LC tissue volumes predicted by the G&R algorithm at normal (0.7 nl) and elevated IOP (1.06 nl) are in very good agreement with the range of volumes (0.49 nl to 1.15 nl) obtained from three-dimensionally reconstructed human LCs by Sigal et al. (2010). Roberts et al. (2009) reported that the connective tissue volume in early glaucoma monkey eyes compared to contralateral normals increased significantly (82%, 44% and 45%) but the average connective tissue volume fraction changed little (-7%, 1% and -2%). The significant increase in collagen fibril volume (63%) and the little change in collagen fibril volume fraction (8%) due to IOP elevation predicted by the G&R simulation are consistent with these experimental results. Yang et al. (2007) observed for three monkeys the consistent thickening of the LC during the earliest stages of experimental glaucoma (59%, 18% and 31%). The numerically predicted thickening of the LC at its center (50%) and at the LC insertion (30.5%) is reasonably close to this experimental evidence.

Our finding of biomechanically-triggered migration of the LC insertion into the sclera and pia may appear surprising to some since for many years it was believed that the LC only inserted into the sclera. Yang et al. (2010) recently observed the outward migration of the posterior lamina insertion point in 9 early experimental glaucoma monkey eyes compared to

their contralateral normal eyes. 3 out of the 9 early experimental glaucoma eyes demonstrated an outward migration of the anterior lamina insertion point such that the LC inserted into the pia. LC insertion into the pia has also been shown to occur in humans (Sigal et al., 2010), although the extent to which this is due to remodeling is still unknown. Yang et al. (2010) also show that the anterior LC surface migrated outwardly but was less pronounced than the migration of the posterior insertion point. The numerical model predicted the outward migration of the posterior lamina insertion point consistent with these experimental observations. In contrast to the experimental observation, the G&R simulation showed an inward migration of the anterior lamina insertion point. This inconsistency indicates that there may be additional factors, such as the biological availability of nutrients or growth factors, that need to be incorporated into the G&R algorithm to capture all aspects of the LC morphologic changes seen in early experimental glaucoma.

The presented simulation is based on a generic human eye model and is a first approach to present a biomechanical explanation of the LC thickening seen in early experimental glaucoma in the monkey. At the present time, very few experimental studies have investigated the mechanisms of laminar G&R during the early stages of glaucoma, and all those studies have been performed in monkeys. The changes reported in the monkey model of glaucoma occurred in 2–9 weeks following exposure to chronic IOP elevations (Yang et al., 2007, 2011, 2010; Roberts et al., 2009), yet the development of glaucoma in humans generally takes years. No data is available for LC remodeling in the earliest stages of glaucoma in humans, hence the results presented herein are representative of the G&R process that is likely to occur in human eyes. In addition, the numerical simulation in which the LC is created by the G&R algorithm does not represent an embryologically accurate development process, but it does support the notion that the LC is necessary in human eyes to resist the mechanical effects of IOP on the neural canal tissues.

The LC-like structure created by the G&R algorithm at normal IOP developed at the posterior end of the scleral canal and partially inserted into the pia matter. The insertion of the LC into the pia is present in some ostensibly normal human eyes (Sigal et al., 2010) and is likely to move posteriorly via a remodeling process in eyes with elevated IOP (Downs et al., 2010). The predicted position of the LC insertion at normal IOP relates to the assumed initial conditions of the model including the eye geometry, constitutive parameters and the collagen fibril architecture. In particular, different eye diameters might lead to different collagen fibril density predictions in the neural canal tissues. For a given IOP, larger globes would lead to a higher mechanical loading of the neural canal tissues. In this case, the G&R algorithm would predict a thicker LC. Conversely, smaller globes in animals such as in rodents would lead to a lower mechanical stress, which in turn might not require the existence of a LC to resist the IOP imposed stress in the ONH. Still, predicting the effects of a single parameter, such as globe size, on the biomechanics of the ONH is complicated because the model parameters interact (Sigal et al., 2005; Sigal, 2009) as well as the remodeling mechanisms (Grytz et al., 2011). We plan on using parametric analysis techniques to assess the influence of inter-species eye differences on the biomechanical need for an LC-like collagenous structure spanning the scleral canal.

Glaucoma is generally associated with cupping of the ONH surface, which is clinically visible using a variety of instruments (Hernandez, 2000; Jonas et al., 2003; Ren et al., 2009). There are two components of glaucomatous cupping; the first is prelaminar cupping due to the loss of prelaminar neural tissues as axons die, and the second is LC excavation that is due to the remodeling of the LC into a more posteriorly deformed structure (Yang et al., 2007; Burgoyne and Downs, 2008; Downs et al., 2008, 2010; Yang et al., 2011). While it is unclear how extensive the LC excavates in human glaucoma, LC excavation has been shown to accompany LC thickening in early experimental glaucoma in the non-human primate

(Yang et al., 2007, 2011). The G&R simulation results presented herein do not predict significant LC excavation at elevated IOP. Parametric studies have shown that the magnitude of acute IOP-induced LC excavation depends on several characteristics of the tissues of the ONH, both geometric and constitutive (Sigal et al., 2011). A different amount of LC excavation may be predicted for a different set of model parameters. Still, there may be additional factors that need to be incorporated into the algorithm to fully capture the glaucomatous changes in LC morphology.

Based on a microstructure-motivated constitutive formulation for crimped collagen fibrils, the G&R stimulus was traced back to the collagen fibril stretch based on recent experimental evidence of collagen fibril degradation mechanisms (Flynn et al., 2010). In contrast to classical G&R approaches based on macroscopic strain or stretch stimuli, the microstructure-motivated stimulus proposed here decouples geometric effects, such as collagen fibril uncrimping and residual strains, from the hypothesized homeostatic biomechanical state. Previous G&R formulations also incorporated a residual stretch (also called recruitment stretch) to motivate a homeostatic mechanical state at the collagen fiber level (Watton et al., 2009a; Machyshyn et al., 2010). These models required for a rather high homeostatic stretch value (also called attachment stretch) $\lambda_{\text{hom}}=1.1$ to achieve a realistic G&R response. Latest experimental results, however, suggest that collagen fibrils experience much lower prestretch (attachment stretch) levels after synthesis. The experiments also suggest for a much lower protective or homeostatic stretch level than 1.1 (Camp et al., 2011). Incorporation of the collagen fibril crimp response in addition to the residual stretch enables the present formulation to use a more realistic (low) value for the homeostatic stretch at the fibril level $\lambda_{\text{hom}}=1.001$.

At elevated IOP, the maximum residual stretch values localized at the region where the LC, pia and sclera meet. This region of the neural canal is characterized by an IOP-induced strain concentration. While the major structural effect during the early glaucoma G&R simulation was achieved by controlling collagen fibril synthesis and degradation, homeostasis in this region was only achieved when the adaptation of both the collagen fibril mass and the residual stretch was considered.

We acknowledge that the tissue can grow and remodel in every direction. Soft tissue G&R, however, is often classified into tissue thickening/thinning or elongation/shortening because these two phenomena are taken to have two different etiologies. Hence, we assumed that tissue thickening/thinning was a growth-based phenomenon represented here by a transverse isotropic growth tensor at the macro-scale. In contrast, tissue elongation/shortening was assumed to be a remodeling phenomenon represented by the adaptation of the residual stretch in accordance with the experimental findings of Foolen et al. (2010). Note that tissue elongation/shortening can also be computationally modeled by using a growth tensor based formulation (see Göktepe et al., 2010).

While the G&R stimulus is derived from the tissue microstructure, the parameters that control the rate of the G&R process (τ_R, τ_g) including the limiting growth factors ($J_{g,min}^{\text{col}}, J_{g,max}^{\text{col}}$) are phenomenologically based and do not have a clear biological interpretation. Further development should explicitly address growth factors, enzyme and nutrients concentrations, and signaling pathways that control the maintenance of the collagen fibril architecture.

It is important to note that the choice of the evolution laws, in particular the choice of the stimulus and model parameters that control the evolution of the residual stretch and the evolution of the growth Jacobian, have particular consequences on the numerical results.

Parametric analyses are needed to reveal the sensitivity of the two proposed biomechanically-driven mechanisms on the G&R simulation.

Mixture theory was applied to derive the change in bulk LC tissue volume and stiffness from the changing volume of collagen fibrils. The present model cannot be used to localize the changing biomechanical environment of the axon bundles at the micro-scale, such as a potential compression of the axon bundles due to new collagen fibril material. To obtain localized information of the biomechanical environment of the axon bundles at the micro-scale, computational coupled finite element simulations at multiple scales might be applied as suggested in Grytz (2008). Numerical G&R simulations at multiple scales can be of great value to gain insight into the biomechanical phenomena related to the glaucomatous damage of the axon bundles, but that is beyond the scope of this paper.

In conclusion, the G&R algorithm presented herein provided evidence in support of the biomechanical need for a LC in humans. The numerical results suggest that IOP elevation may lead to LC thickening due to an increase in collagen fibril mass and due to the recruitment of pre- and retro-laminar tissues into the LC, which is in good agreement with latest experimental observations in early glaucoma monkey eyes. This is the first study to demonstrate that a biomechanically-driven G&R mechanism can lead to the characteristic thickening of the LC seen in early glaucoma.

References

- Ambrosi D, Ateshian GA, Arruda EM, Cowin SC, Dumais J, Goriely A, Holzapfel GA, Humphrey JD, Kemkemer R, Kuhl E, Olberding JE, Taber LA, Garikipati K. Perspectives on biological growth and remodeling. *J. Mech. Phys. Solids*. 2011; 59:863–883. [PubMed: 21532929]
- Bhole AP, Flynn BP, Liles M, Saeidi N, Dimarzio CA, Ruberti JW. Mechanical strain enhances survivability of collagen micronetworks in the presence of collagenase: implications for load-bearing matrix growth and stability. *Philos Transact A Math Phys Eng Sci*. 2009; 367:3339–3362. [PubMed: 19657003]
- Burgoyne CF, Downs JC. Premise and prediction—how optic nerve head biomechanics underlies the susceptibility and clinical behavior of the aged optic nerve head. *J. Glaucoma*. 2008; 17:318–328. [PubMed: 18552618]
- Camp RJ, Liles M, Beale J, Saeidi N, Flynn BP, Moore E, Murthy SK, Ruberti JW. Molecular mechanochemistry: low force switch slows enzymatic cleavage of human type I collagen monomer. *J. Am. Chem. Soc*. 2011; 133:4073–4078. [PubMed: 21348512]
- Downs JC, Roberts MD, Burgoyne CF. Mechanical environment of the optic nerve head in glaucoma. *Optom. Vis. Sci*. 2008; 85:425–435. [PubMed: 18521012]
- Downs JC, Roberts MD, Sigal IA. Glaucomatous cupping of the lamina cribrosa: A review of the evidence for active progressive remodeling as a mechanism. *Exp. Eye. Res*. 2010 (in press).
- Epstein M, Maugin GA. Thermomechanics of volumetric growth in uniform bodies. *Int. J. Plasticity*. 2000; 16:951–978.
- Flynn BP, Bhole AP, Saeidi N, Liles M, Dimarzio CA, Ruberti JW. Mechanical strain stabilizes reconstituted collagen fibrils against enzymatic degradation by mammalian collagenase matrix metalloproteinase 8 (MMP-8). *PLoS ONE*. 2010; 5:e12337. [PubMed: 20808784]
- Foolen J, van Donkelaar CC, Soekhradj-Soeichit S, Ito K. European society of biomechanics s.m. perren award 2010: An adaptation mechanism for fibrous tissue to sustained shortening. *J. Biomech*. 2010; 43:3168–3176. [PubMed: 20817184]
- Girard MJA, Downs JC, Bottlang M, Burgoyne CF, Suh JF. Peripapillary and posterior scleral mechanics—Part II: Experimental and inverse finite element characterization. *J. Biomech. Eng*. 2009; 131:051012. [PubMed: 19388782]
- Göktepe S, Abilez OJ, Parker KK, Kuhl E. A multi-scale model for eccentric and concentric cardiac growth through sarcomerogenesis. *J. Theor. Biol*. 2010; 265:433–442. [PubMed: 20447409]

- Grytz, R. Ph.D. thesis. Ruhr-University Bochum; Germany: 2008. Computational Modeling and Remodeling of Human Eye Tissues as Biomechanical Structures at Multiple Scales..
- Grytz R, Meschke G. Constitutive modeling of crimped collagen fibrils in soft tissues. *J. Mech. Behavior Biomed. Mat.* 2009; 2:522–533.
- Grytz R, Meschke G. A computational remodeling approach to predict the physiological architecture of the collagen fibril network in corneo-scleral shells. *Biomech. Model. Mechanobiol.* 2010; 9:225–235. [PubMed: 19802726]
- Grytz R, Meschke G, Jonas JB. The collagen fibril architecture in the lamina cribrosa and peripapillary sclera predicted by a computational remodeling approach. *Biomech. Model. Mechanobiol.* 2011; 10:371–382. [PubMed: 20628781]
- Hernandez MR. The optic nerve head in glaucoma: Role of astrocytes in tissue remodeling. *Progr. Ret. Eye Res.* 2000; 19:297–321.
- Hernandez MR, Luo XX, Igoe F, Neufeld AH. Extra-cellular matrix of the human lamina cribrosa. *Am. J. Ophthalmol.* 1987; 104:567–576. [PubMed: 3318474]
- Himpel G, Kuhl E, Menzel A, Steinmann P. Computational modelling of isotropic multiplicative growth. *Comput. Model. Eng. Sci.* 2005; 8:119–134.
- Jonas JB, Berenshtein E, Holbach L. Anatomic relationship between lamina cribrosa, intraocular space and cerebrospinal fluid space. *Invest. Ophthalmol. Vis. Sci.* 2003; 44:5189–5195. [PubMed: 14638716]
- Klisch SM, Chen SS, Sah RL, Hoger A. A growth mixture theory for cartilage with application to growth-related experiments on cartilage explants. *J. Biomech. Eng.* 2003; 125:169–179. [PubMed: 12751278]
- Kuhl E, Maas R, Himpel G, Menzel A. Computational modeling of arterial wall growth. attempts towards patient-specific simulations based on computer tomography. *Biomech. Model. Mechanobiol.* 2007; 6:321–331. [PubMed: 17119902]
- Kuhl, E.; Steinmann, P. Mass- and volume-specific views on thermodynamics for open systems; Proceedings of the Royal Society of London. Series A: Mathematical, Physical and Engineering Sciences; 2003. p. 2547-2568.
- Laurent GJ, McAnulty RJ, Gibson J. Changes in collagen synthesis and degradation during skeletal muscle growth. *Am. J. Physiol.* 1985; 249:C352–C355. [PubMed: 4037076]
- Laurent GJ, Sparrow MP, Bates PC, Millward DJ. Turnover of muscle protein in the fowl. collagen content and turnover in cardiac and skeletal muscles of the adult fowl and the changes during stretch-induced growth. *Biochem. J.* 1978; 176:419–427. [PubMed: 743250]
- Lubarda VA, Hoger A. On the mechanics of solids with a growing mass. *Int. J. Solids Struct.* 2002; 39:4627–4664.
- Machyshyn IM, Bovendeerd PHM, van de Ven AAF, Rongen PMJ, van de Vosse FN. A model for arterial adaptation combining microstructural collagen remodeling and 3D tissue growth. *Biomech. Model. Mechanobiol.* 2010; 9:671–687. [PubMed: 20300950]
- Morrison JC, L'Hernault NL, Jerdan JA, Quigley HA. Ultrastructural location of extracellular matrix components in the optic nerve head. *Arch. Ophthalmol.* 1989; 107:123–129. [PubMed: 2910271]
- Ren R, Wang N, Li B, Li L, Gao F, Xu X, Jonas JB. Lamina cribrosa and peripapillary sclera histomorphometry in normal and advanced glaucomatous chinese eyes with various axial length. *Invest. Ophthalmol. Vis. Sci.* 2009; 50:2175–2184. [PubMed: 19387083]
- Roberts MD, Grau V, Grimm J, Reynaud J, Bellezza AJ, Burgoyne CF, Downs JC. Remodeling of the connective tissue microarchitecture of the lamina cribrosa in early experimental glaucoma. *Invest. Ophthalmol. Vis. Sci.* 2009; 50:681–690. [PubMed: 18806292]
- Rodriguez EK, Hoger A, McCulloch AD. Stress-dependent finite growth in soft elastic tissues. *J. Biomech.* 1994; 27:455–467. [PubMed: 8188726]
- Schmid H, Pauli L, Paulus A, Kuhl E, Itskov M. Consistent formulation of the growth process at the kinematic and constitutive level for soft tissues composed of multiple constituents. *Comput. Meth. Biomech. Biomed. Eng.* 2011 (in press).
- Sigal IA. Interactions between geometry and mechanical properties on the optic nerve head. *Invest. Ophthalmol. Vis. Sci.* 2009; 50:2785–2795. [PubMed: 19168906]

- Sigal IA, Flanagan JG, Ethier CR. Factors influencing optic nerve head biomechanics. *Invest. Ophthalmol. Vis. Sci.* 2005; 46:4189–4199. [PubMed: 16249498]
- Sigal IA, Flanagan JG, Tertinegg I, Ethier CR. 3D morphometry of the human optic nerve head. *Exp. Eye. Res.* 2010; 90:70–80. [PubMed: 19772858]
- Sigal IA, Yang H, Roberts MD, Burgoyne CF, Downs JC. IOP-induced lamina cribrosa displacement and scleral canal expansion: an analysis of factor interactions using parameterized eye-specific models. *Invest. Ophthalmol. Vis. Sci.* 2011; 52:1896–1907. [PubMed: 20881292]
- Wang JH, Thampatty BP. An introductory review of cell mechanobiology. *Biomech. Model. Mechanobiol.* 2006; 5:1–16. [PubMed: 16489478]
- Watton PN, Raberger NB, Ventikos Y, A. H.G. Coupling the haemodynamic environment to the growth of cerebral aneurysms: Computational framework and numerical examples. *J. Biomech. Eng.* 2009a; 131:101003. [PubMed: 19831473]
- Watton PN, Ventikos Y, Holzapfe GA. Modelling the growth and stabilization of cerebral aneurysms. *Math. Med. Biol.* 2009b; 26:133–164. [PubMed: 19234094]
- Winkler M, Jester B, Nien-Shy C, Massei S, Minckler DS, Jester JV, Brown DJ. High resolution three dimensional reconstruction of the collagenous matrix of the human optic nerve head. *Brain. Res. Bul.* 2010; 81:339–348.
- Woo SL, Kobayashi AS, Lawrence C, Schlegel WA. Mathematical model of the corneo-scleral shell as applied to intraocular pressure-volume relations and applanation tonometry. *Ann. Biomed. Eng.* 1971; 1:87–98. [PubMed: 4668693]
- Yang H, Downs JC, Girkin C, Sakata L, Bellezza A, Thompson H, Burgoyne CF. 3-D histomorphometry of the normal and early glaucomatous monkey optic nerve head: lamina cribrosa and peripapillary scleral position and thickness. *Invest. Ophthalmol. Vis. Sci.* 2007; 48:4597–460. [PubMed: 17898283]
- Yang H, Thompson H, Roberts MD, Sigal IA, Downs JC, Burgoyne CF. Deformation of the early glaucomatous monkey optic nerve head connective tissue following acute iop elevation within 3-D histomorphometric reconstructions. *Invest. Ophthalmol. Vis. Sci.* 2011; 52:345–363. [PubMed: 20702834]
- Yang H, Williams G, Downs JC, Sigal IA, Roberts M, Grimm J, Thompson H, Burgoyne CF. Optic nerve head (ONH) lamina cribrosa insertion migration and pialization in early non-human primate (NHP) experimental glaucoma. *ARVO Abstract.* 2010; 51:1631.
- Yang JL, Neufeld AH, Zorn MB, Hernandez MR. Collagen type i mRNA levels in cultured human lamina cribrosa cells: effects of elevated hydrostatic pressure. *Exp. Eye. Res.* 1993; 56:567–574. [PubMed: 8500565]

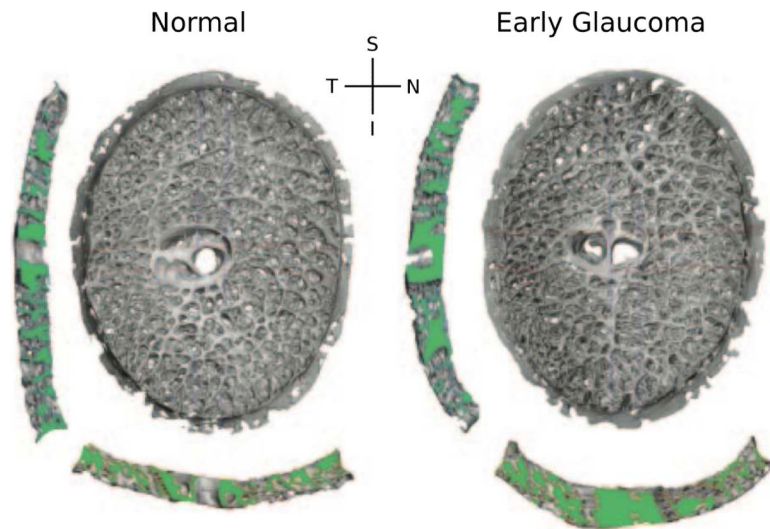


Figure 1. 3D reconstructions of the LC connective tissues of a monkey, with one eye having early experimental glaucoma. Shown are en face views of the lamina reconstructions, as well as views of the central vertical (left) and horizontal (below) sections. Note the thicker and deeper cupped lamina in the early glaucoma eye (adapted from Roberts et al., 2009).

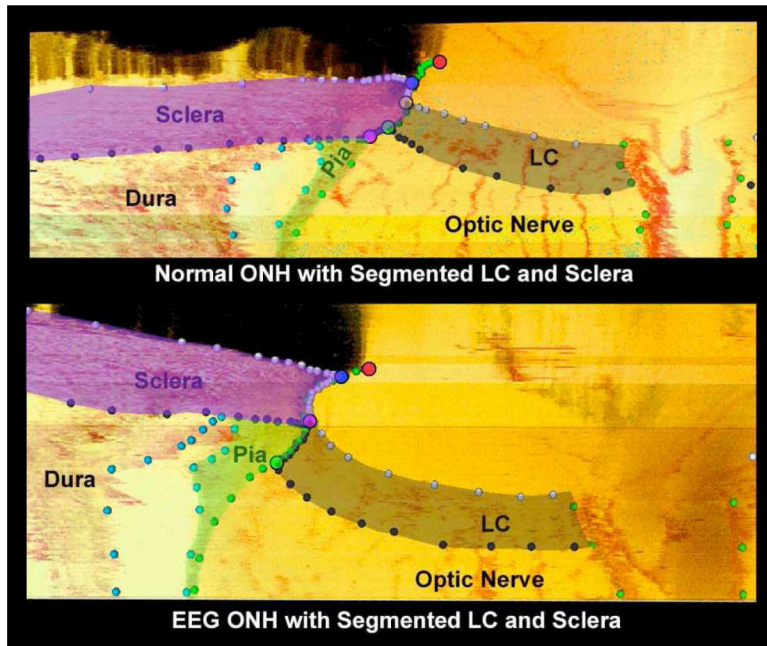


Figure 2. Histologic sections through the ONH with segmented LC and scleral tissues of a monkey, with one eye having early experimental glaucoma (EEG). Note the dedicated outward migration of the LC and its full insertion into the pia in the early glaucoma eye (adapted from Yang et al., 2010).

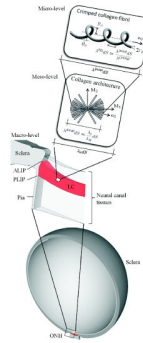
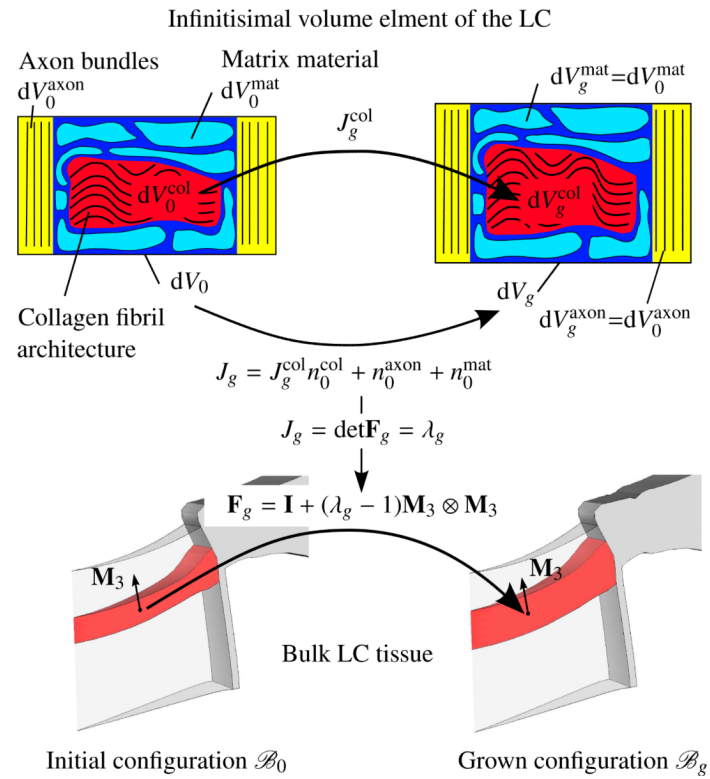


Figure 3.

Micro-level: the crimped collagen fibril; meso-level: the collagen architecture represented by distributed collagen fibril orientations \mathbf{e}_0 ; macro-level: the human eye model (adapted from Sigal, 2009) and the ONH region. Due to residual stretch λ_R , the stretch level in the axial direction of the collagen fibril λ^{axial} can be higher or lower compared to macroscopic elastic stretch λ_e . Due to collagen fibril crimping λ^{crimp} , the absolute elastic strain experienced by the collagen fibril material $|\lambda^{\text{fib}} - 1|$ is always lower compared to the strain in the fibril's axial direction $|\lambda^{\text{axial}} - 1|$. ALIP—anterior lamina insertion point; PLIP—posterior lamina insertion point.

**Figure 4.**

Top: the volumetric growth of the collagen fibril architecture J_g^{col} leads to the volume increase J_g of the bulk LC tissue element from dV_0 to dV_g . Bottom: kinematic thickening of the LC defined by the growth tensor \mathbf{F}_g . The growth multiplier λ_g is linked to the overall volume increase J_g through the determinant of the growth tensor.

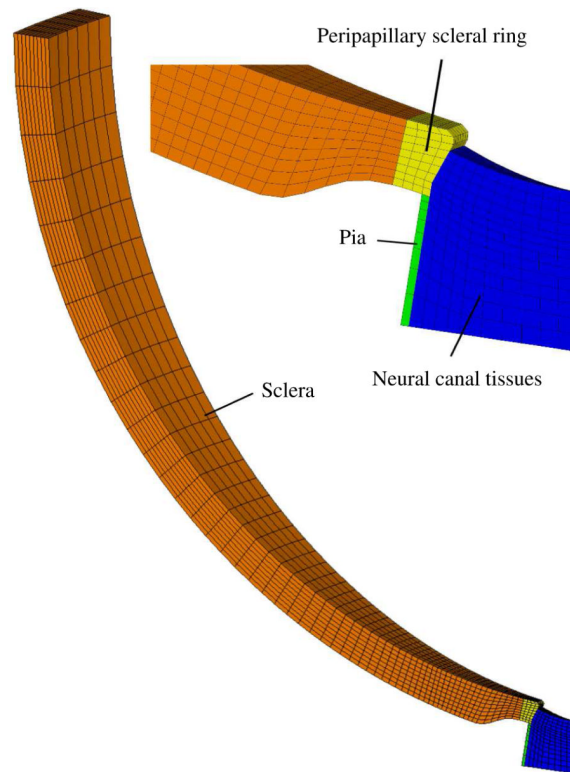


Figure 5. Finite element mesh of the generic axisymmetric model including a detailed view of the ONH region showing the peripapillary sclera, the peripapillary scleral ring tissue, the pia mater and the neural canal tissues.

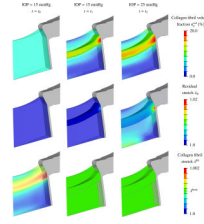


Figure 6.

G&R simulation results showing the neural canal tissues, the peripapillary sclera, the pia matter, and the evolution of the LC at time $t = t_0, t_1, t_2$. Left column ($t = t_0$): model with initial uniform collagen content throughout the tissues within the neural canal subjected to normal IOP (15 mmHg). Middle column ($t = t_1$): model homeostasis at normal IOP (15 mmHg). Right column ($t = t_2$): model homeostasis after IOP elevation (25 mmHg).

Evolution of (top row) the collagen fibril volume fraction n_g^{col} , (middle row) the residual stretch λ_R ; and (bottom row) the collagen fibril stretch λ^{fib} . The surfaces of the LC were defined as those that enclose the neural canal tissue volume with a collagen fibril volume fraction n_g^{col} of 10% or more.

Table 1

Global constitutive parameters of the strain energy functions (SEF) W^{mat} and W^{col} used in (19). The micro-structural and material parameter were adapted from our previous parameter fitting (Grytz, 2008) to inflation experiments performed by Woo et al. (1971) on scleral segments. The material parameters E and μ were modified from the original fitting to account for the volume fraction concept used in the present paper.

SEF	Parameter	Value
W^{mat}	Shear modulus of the matrix material per d V_0^{mat}	$\mu = 0.05$ MPa
W^{col}	Elastic modulus of collagen fibrils per d V_0^{col}	$E = 62.4$ MPa
W^{col}	Collagen fibril crimp angle *	$\theta_0 = 5.09^\circ$
W^{col}	Ratio between the radii of the helix and fibril *	$R_0/r_0 = 1.04$

* Illustrated in Figure 3 (micro-level).

Table 2

Initial volume fractions.

Tissue	n_0^{col}	n_0^{mat}	n_0^{axon}
Sclera	0.6	0.4	0.0
Pia	0.6	0.4	0.0
Neural canal tissues	0.06*	0.235	0.705

* Note that the neural canal tissues were not assumed to have a LC at the initial configuration \mathcal{B}_0 .

Table 3

Structural changes in the LC due to IOP elevation from 15 mmHg to 25 mmHg predicted by the G&R simulation. The LC was defined as neural canal tissue with a collagen fibril volume fraction n_g^{col} of 10% or more.

	IOP		Change
	15 mmHg	25 mmHg	
Bulk tissue volume	0.70 μl	1.06 μl	52%
Total collagen fibril volume	95 nl	155 nl	63%
Overall collagen fibril volume fraction	13.7%	14.8%	8%
LC central thickness	167 μm	250 μm	50%
LC thickness at scleral insertion	275 μm	359 μm	30.5%